CrossMark

CLINICAL STUDY

# In vivo molecular profiling of human glioma using diffusion kurtosis imaging

Johann-Martin Hempel[1] · Sotirios Bisdas[1,2] · Jens Schittenhelm[3] ·
Cornelia Brendle[1] · Benjamin Bender[1] · Henk Wassmann[1] · Marco Skardelly[4] ·
Ghazaleh Tabatabai[5] · Salvador Castaneda Vega[6] · Ulrike Ernemann[1] · Uwe Klose[1]

**Abstract** The purpose of this study is to assess the diagnostic performance of diffusion kurtosis imaging (DKI) for in vivo molecular profiling of human glioma. Normalized mean kurtosis ($MK_n$) and mean diffusivity ($MD_n$) metrics from DKI were assessed in 50 patients with histopathologically confirmed glioma. The results were compared in regard to the WHO-based histological findings and molecular characteristics leading to integrated diagnosis (Haarlem Consensus): isocitrate-dehydrogenase (IDH1/2) mutation status, alpha-thalassemia/mental retardation syndrome X-linked (ATRX) expression, chromosome 1p/19q loss of heterozygosity (LOH), and O6-methylguanine DNA methyltransferase (MGMT) promoter methylation status. $MK_n$ was significantly lower in tumors with IDH1/2 mutation ($0.43 \pm 0.09$) and ATRX loss of expression ($0.41 \pm 0.11$) than in those with IDH1/2 wild type ($0.57 \pm 0.09$, $p < 0.001$) and ATRX maintained expression ($0.51 \pm 0.10$, $p = 0.004$), respectively. Regarding the integrated molecular diagnosis, $MK_n$ was significantly higher in primary glioblastoma ($0.57 \pm 0.10$) than in astrocytoma ($0.39 \pm 0.11$, $p < 0.001$) and oligodendroglioma ($0.47 \pm 0.05$, $p = 0.003$). MK may be used to provide insight into the human glioma molecular profile regarding IDH1/2 mutation status and ATRX expression. Considering the diagnostic and prognostic significance of these molecular markers, MK appears to be a promising in vivo biomarker for glioma. The diagnostic performance of MK seems to fit more with the integrated molecular approach than the conventional histological findings of the current WHO 2007 classification.

**Keywords** Diffusion kurtosis imaging · Glioma · Isocitrate dehydrogenase · IDH1/2 · ATRX · 1p/19q LOH · MGMT · Integrated diagnosis · Haarlem consensus

The original version of this article was revised: The second author's family name was incorrect. The name has been updated in this version.

✉ Johann-Martin Hempel
johann-martin.hempel@uni-tuebingen.de

1  Department of Neuroradiology, Eberhard Karls University, Tübingen, Germany

2  Department of Neuroradiology, National Hospital of Neurology and Neurosurgery, University College London Hospitals, London, UK

3  Institute of Neuropathology, Eberhard Karls University, Tübingen, Germany

4  Department of Neurosurgery, Eberhard Karls University, Tübingen, Germany

5  Centre of Neurooncology, Comprehensive Cancer Center Tübingen-Stuttgart, Eberhard Karls University, Tübingen, Germany

6  Department of Preclinical Imaging and Radiopharmacy, Werner Siemens Imaging Center, Eberhard Karls University, Tübingen, Germany

## Introduction

The WHO classifies tumors of the central nervous system based on histopathological criteria that are associated with the degree of biological aggressiveness and expected clinical outcome. These criteria include cellular atypia (diffuse astrocytoma grade II, AS2), anaplasia and mitotic activity (anaplastic astrocytoma grade III, AS3), and microvascular proliferation or necrosis (GBM) [1]. Accurately grading glioma is important for the prognosis and management of clinical pathways [1, 2]. Histologic examination has been essential for definitive grading of glioma because non-invasive imaging methods

suffer from low specificity [3–5]. However, reliable and robust non-invasive tumor grading is important for optimal care of patients who cannot be treated surgically, who have high risk of post-biopsy complication, or for regular follow-up of low-grade glioma [6, 7].

The diffusion displacement probability distribution is Gaussian in a homogeneous liquid such as water [8, 9], but it deviates considerably from a Gaussian distribution in complex cellular structures such as brain tissue [9]. Also known as the apparent excess kurtosis coefficient (AKC), the excess diffusional kurtosis (DK) is a dimensionless metric that quantifies the degree of deviation from Gaussian diffusion behavior [10]. DK imaging (DKI) can be used to describe the degree of structure of a biological tissue [9–11]. As an extension of the diffusion tensor (DT) imaging model, DKI allows for simultaneous direction-dependent estimation of the apparent diffusion coefficient (ADC) and AKC [12].

DKI has been applied to glioma to enable non-invasive tumor grading by providing additional information on microstructural features and microdynamics [2, 6, 13]. This promising method allows for better discrimination than conventional diffusion parameters or morphological imaging between different glioma grades (WHO grades II–IV) [13, 14] as well as between high-grade and low-grade glioma [2, 6, 14, 15]. Furthermore, the combination of DKI and other advanced magnetic resonance (MR) imaging methods such as MR perfusion imaging or chemical shift imaging shows promise for increasing the diagnostic accuracy of tumor grade differentiation [6].

However, the value of DKI has not yet been sufficiently investigated in the context of the upcoming integrated diagnostic approach for adult glioma, which combines histological and molecular tumor data into an integrated diagnosis (ID) according to the International Society of Neuropathology—Haarlem consensus guidelines [16–19]. Preliminary results suggest that DKI has potential for non-invasive prognosis of cellular proliferation [14]. Therefore, this study aims to assess the diagnostic capabilities of DKI for grading glioma according to the relevant prognostic molecular characteristics leading to integrated molecular diagnosis (Haarlem consensus). These characteristics include isocitrate-dehydrogenase (IDH) mutation status, alpha-thalassemia/mental retardation syndrome X-linked (ATRX) expression, chromosome 1p/19q loss of heterozygosity (LOH), and O6-methylguanine DNA methyltransferase (MGMT) promoter methylation status.

## Materials and methods

### Study design and ethics

The present study is a retrospective analysis of prospective data acquired in a single-center, non-randomized trial, which was approved by the local institutional review board of our university hospital. The trial was conducted based on the principles of the International Conference on Harmonisation of Good Clinical Practice guidelines and according to the revised version of the Declaration of Helsinki. All patients provided written informed consent for the imaging surveys and the subsequent use of images for scientific and research purposes.

### Study group and validity

The study group was selected from 61 consecutive patients comprising 31 males and 30 females with a mean age of $50.1 \pm 14.3$ years (range 19–80 years). These patients were referred to our hospital between October 2012 and March 2016 with head MRI scans and symptoms that suggested a cerebral mass. One inclusion criterion for the study was tumors of potential glial origin with indeterminate findings in conventional MRI for tumor grading (absent or faint/scattered gadolinium enhancement, extensive edema or gliosis, no necrosis or hemorrhage). Other criteria were the patient's informed consent for an advanced multimodal imaging exam and stereotactic histological sampling of the tumor area. All studies were completed within 2 weeks of diagnosis and before initiating treatment. None of the patients received steroid treatments at the time of analysis.

General exclusion criteria were any contraindications for MR exams as well as agitated and non-cooperating patients. Of the original 61 patients, 11 were excluded because they were lost to follow-up (n=3), they did not undergo any histological sampling of the diagnosed cerebral lesion (n=5), the imaging data was corrupt (n=2), or they stopped the examination early because of claustrophobia (n=1).

The final study group included 50 patients with a mean age of $49.9 \pm 14.2$ years (range 25–80 years) and comprised 24 men (48%) and 26 women (52%). Among these patients, 16 (32%) had suspected recurrent glioma. The final diagnosis was based on histological examinations of specimens obtained by biopsy in all patients, followed by partial or complete tumor resection in 39 patients (78%).

Histological findings were classified according to the current WHO 2007 classification criteria [1]. In the context of an integrated diagnostic approach for adult astrocytoma, oligodendroglioma, and glioblastoma, the examined tumors were also classified according to their molecular characteristics, which is expected in the upcoming WHO revision [16–20]. In particular, IDH mutation status was assessed by immunohistochemistry with a mutation-specific IDH1 R132H antibody [21, 22]. This was followed by Sanger sequencing of the negative cases to detect any non-canonical IDH1/2 mutations [23]. Nuclear ATRX status in tumor cells was determined by immunohistochemistry as previously described [18]. A synthetic high-resolution gel was used to study chromosome 1p/19q LOH in all tumors

with an oligodendroglial component [24]. MGMT status was assessed by methylation-specific PCR in all high-grade tumors [19, 25]. Histology and molecular data were combined into an "integrated diagnosis" according to the International Society of Neuropathology—Haarlem Consensus Guidelines [16]. Additionally, staining for MIB-1 (anti–Ki-67, clone MIB-1, dilution 1:200, Dako, Billeria CA) was performed on the Benchmark immunohistochemistry system with following OptiView settings: Cell conditioner 1 pretreatment for 40 min, primary antibody incubation for 20 min at 42 °C.

## Procedures and techniques

### MRI imaging

Imaging was performed using a 3.0 T MRI scanner (Biograph mMR, Siemens Healthcare, Erlangen, Germany). The conventional MR examination protocol included a transversal 2D-encoded T2-weighted fluid attenuated inversion recovery (FLAIR) sequence (TR/TE, 9000/87 ms; inversion time (TI), 2500 ms; slice number, 40; slice thickness, 3 mm), a T2-weighted 2D-encoded fast spin-echo (FSE) sequence in sagittal and coronal orientations (TR/TE, 5000/90 ms; slice number, 32; slice thickness, 3 mm), and a sagittal 3D-encoded isotropic magnetization prepared rapid acquisition gradient echo (MPRAGE) sequence (TR/TE, 1900/2.4 ms; TI, 900 ms; slice number, 124; slice thickness, 1.0 mm) before and after contrast agent administration (0.1 ml/kg body weight gadobutrol).

The DKI protocol has been described in previous reports [12, 13]. A spin-echo echo-planar imaging DW imaging sequence was used for the process. The $b$ values implemented were 0, 500, 1000, 1500, 2000, and 2500 s/mm$^2$ according to previous studies [9, 11, 13]. Diffusion encoding in 30 directions was used for each of these values. The other imaging parameters were as follows: TR 5900 ms, TE 95 ms; field of view $250 \times 250$ mm$^2$; matrix $128 \times 128$; slice number, 25, slice thickness, 5 mm; bandwidth, 965 Hz/pixel; parallel imaging with a sensitivity encoding factor of two in the anteroposterior direction.

### Image post-processing

The image post-processing algorithm has been described previously [12]. Three-dimensional motion correction and spatial smoothing (Gaussian filter with full width at half maximum of 1.0 mm) were performed on the diffusion images using the MR Body Diffusion tool® V 1.1.0 in syngo.via frontier® (Siemens Healthcare, Erlangen, Germany). ADC and AKC parametric maps were calculated, and the values of ADC (mean diffusivity, MD) and AKC (mean kurtosis, MK) were obtained as the average of all 30 directions of the six $b$ values.

Image and volume of interest (VOI) analyses were performed on the parametric maps using MIPAV (http://mipav.cit.nih.gov/). The algorithm for VOI analysis has been described previously [13]. First, the anatomic transverse FLAIR-weighted images were co-registered with the ADC and AKC parametric maps using an automatic image registration method based on cost-function optimization. The VOIs were manually drawn on the co-registered images around each whole tumor on multiple slices, indicated by T2 signal alterations (Fig. 1), as well as in the contralateral frontoparietal supraventricular normal-appearing white matter (NAWM). By encompassing the whole tumor, we sought to minimize potential sampling bias [26, 27]. The MK and MD voxel intensity values were then extracted from the overlaid VOIs and exported for statistical analysis.

### Statistical analyses

Data analyses were performed using IBM SPSS Statistics® Version 22 (IBM, Armonk, NY, USA). Given the wide age range of the study patients and the reported age-related changes of MK in white matter [28, 29], a linear regression was performed on the MK and MD values of the NAWM versus age. In order to account for potential inter-individual variations of the brain, the MK and MD data were normalized to the NAWM values of each patient as follows:

(a) $MK_n = MK_{tumor} / MK_{NAWM}$; and
(b) $MD_n = MD_{tumor} / MD_{NAWM}$

The Shapiro–Wilk test for normal distributions was applied for all variables. For each patient, the $MK_n$ and $MD_n$ values were compared between high-grade (HGG) and low-grade glioma (LGG) using the Mann–Whitney U-test. After testing for homogeneous variance with the Levené test, one-way analysis of variance (ANOVA) with post-hoc Scheffé correction was used for comparison between WHO grade II (G2G), grade III (G3G), and grade IV glioma (GBM), as well as between integrated diagnoses of astrocytoma, oligodendroglioma, and glioblastoma. The Mann–Whitney U-test was also used to compare $MK_n$ and $MD_n$ values between tumors with the wild type and mutation of IDH1/2 in all patients and in patients with astroglial brain tumor (AS2, AS3, and GBM). Comparisons were also made between maintained ATRX and loss of expression (LOE), between the wild type and LOH of 1p/19q, and between methylated and unmethylated MGMT promoter. Tests of the seven a priori hypotheses were conducted using Bonferroni adjusted alpha levels of 0.0071 per test (0.05/7).

The Pearson correlation coefficient was used to correlate $MK_n$ values with WHO-based tumor grades and integrated

**Fig. 1** Assessment of metrics from diffusion kurtosis imaging. Measurement of mean kurtosis (MK) and mean diffusivity (MD) metrics from diffusion kurtosis imaging (DKI) in a 38-years old patient with histopathologically confirmed anaplastic astrocytoma WHO grade III with IDH1-R132H mutation. One exemplary slice of the volume of interest (VOI) is drawn around the whole tumor on ADC (**b**, **c**) and AKC (**e**, **f**) parametric maps, based on T2 signal alterations on the co-registered fluid attenuation inversion recovery (FLAIR) sequence (**a**). The tumor shows faint enhancement in contrast-enhanced axial reformatted T1 magnetization prepared rapid acquisition gradient echo (MPRAGE) sequence (**d**)
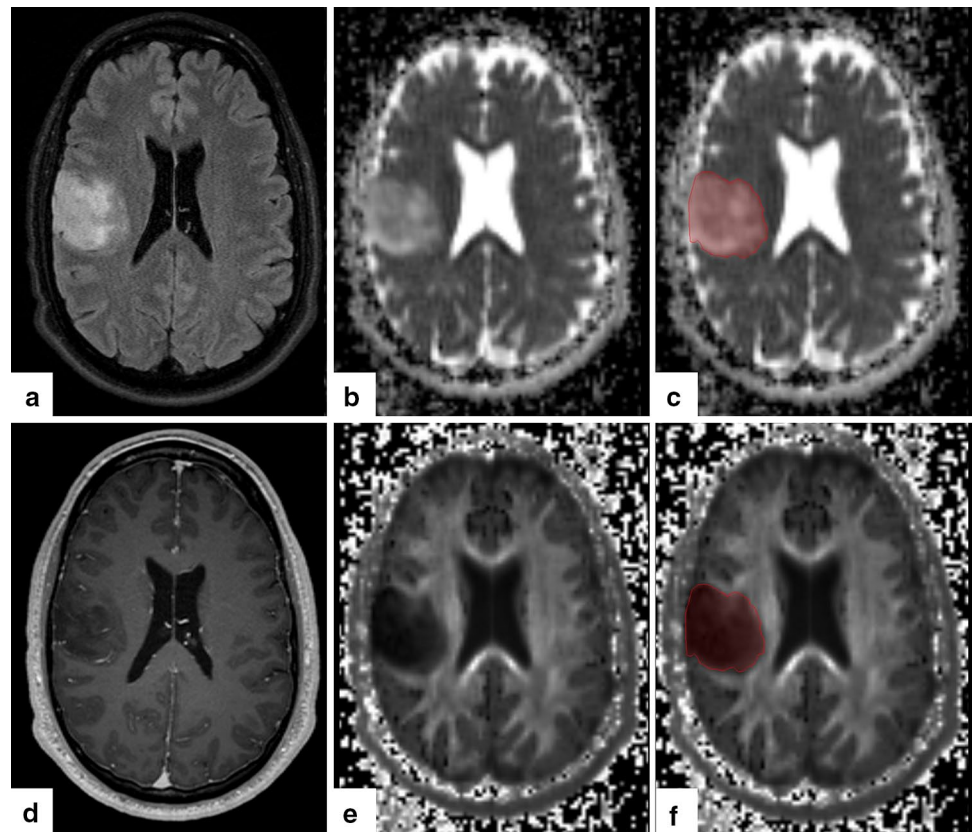


molecular diagnoses, respectively. The Pearson correlation coefficient was also used to correlate MIB-1 values with $MK_n$ and $MD_n$ values.

Receiver operating characteristic (ROC) curves were generated for $MK_n$ for all significant results to determine the area under the curve (AUC). The results with the highest Youden index were defined as the optimal cutoff values.

## Results

Table 1 shows the histological findings according to the current WHO 2007 classification criteria and the integrated diagnosis according to molecular characteristics (Haarlem Consensus).

The linear regression of the average MK values in the NAWM versus age showed a non-significant weakly negative correlation between these parameters and a slight decrease in the MK of the white matter with increasing age ($r_P = -0.185$, $r_P^2 = 0.066$, $\beta = -0.002$, $p = 0.071$). The linear regression of the average MD values in the NAWM versus age showed a non-significant weakly negative correlation and a slight increase of the MD of the white matter with increasing age ($r_P = 0.243$, $r_P^2 = 0.059$, $\beta = 0.001$, $p = 0.108$).

Table 2 shows the average $MK_n$ and $MD_n$ values with the standard deviations of G2G, G3G, GBM, LGG, and

HGG, as well as the integrated diagnoses of astrocytoma, oligodendroglioma, and glioblastoma. The table also shows the results for IDH1/2 mutation, ATRX expression, 1p/19q LOH, and MGMT methylation. The values are illustrated in boxplots in Fig. 2a–h. Among the WHO-based histological findings, $MK_n$ was significantly lower in G2G ($0.41 \pm 0.09$) than in G3G ($0.53 \pm 0.11$; $p = 0.002$) and GBM ($0.52 \pm 0.11$; $p = 0.005$) (Fig. 2a), whereas $MD_n$ was significantly higher in G2G ($1.86 \pm 0.40$) than in G3G ($1.48 \pm 0.33$, $p = 0.007$) (Fig. 2b). GBM could not be differentiated from G3G (Fig. 2a, b). Additionally, $MK_n$ was significantly lower in LGG ($0.41 \pm 0.09$) than in HGG ($0.52 \pm 0.11$; $p < 0.001$), whereas $MD_n$ was significantly higher ($p = 0.002$). For molecular characteristics, $MK_n$ was significantly lower in tumors with IDH1/2 mutation ($0.43 \pm 0.09$) than in those with IDH1/2 wild type ($0.57 \pm 0.09$; $p < 0.001$) (Fig. 2e), whereas $MD_n$ was significantly higher ($p = 0.005$) (Fig. 2f). In subgroup analysis of all patients with astroglial brain tumor (AS2, AS3, and GBM), $MK_n$ was also significantly lower in tumors with IDH1/2 mutation ($0.39 \pm 0.11$) than in those with IDH1/2 wild type ($0.57 \pm 0.10$; $p < 0.001$), whereas $MD_n$ was significantly higher ($p = 0.002$). $MK_n$ was significantly lower in tumors with ATRX LOE ($0.41 \pm 0.11$) than in those with maintained ATRX expression ($0.51 \pm 0.10$; $p = 0.004$) (Fig. 2g), whereas $MD_n$ showed a non-significant tendency towards lower values ($p = 0.072$) (Fig. 2h). There

**Table 1** Tumor grading according to WHO-based histological findings and integrated molecular approach

| WHO 2007-based histological findings (n = 50) | |
|---|---|
| Grade II glioma | n = 25 (50%) |
| Grade III glioma | n = 15 (30%) |
| Grade IV glioblastoma | n = 10 (20%) |
| IDH1/2 mutant glioblastoma | n = 2 (4%) |
| Low grade glioma (II) | n = 25 (50%) |
| High grade glioma (III-IV) | n = 25 (50%) |
| Astrocytoma | n = 22 (44%) |
| Oligodendroglioma | n = 4 (8%) |
| Oligoastrocytoma | n = 14 (28%) |
| Integrated molecular diagnosis (n = 48) | |
| Astrocytoma | n = 19 (39%) |
| Oligodendroglioma | n = 14 (29%) |
| Glioblastoma | n = 15 (31%) |
| IDH1/2 status in all tumors (n = 49) | |
| IDH1/2 wild type | n = 16 (33%) |
| IDH1/2 mutation | n = 33 (67%) |
| IDH1/2 status in AS2, AS3, and GBM (n = 34) | |
| IDH1/2 wild type | n = 15 (44%) |
| IDH1/2 mutation | n = 19 (56%) |
| IDH1/2 mutation type (n = 49) | |
| R132H | n = 30 (61%) |
| R172M | n = 1 (2%) |
| R172K | n = 2 (4%) |
| ATRX expression (n = 45) | |
| Maintained | n = 26 (58%) |
| Loss | n = 19 (42%) |
| Chromosome 1p/19q status (n = 35) | |
| Lack of LOH | n = 18 (51%) |
| Partial LOH | n = 5 (14%) |
| Complete LOH | n = 12 (34%) |
| MGMT promoter (n = 35) | |
| Unmethylated | n = 16 (46%) |
| Methylated | n = 19 (54%) |

*IDH* isocitrate-dehydrogenase, *ATRX* alpha-thalassemia/mental retardation syndrome X-linked expression, *1p/19q LOH* 1p/19q loss of heterozygosity, *MGMT* O6-methylguanine DNA methyltransferase status, *AS2* astrocytoma grade II, *AS3* astrocytoma grade III, *GBM* glioblastoma

**Table 2** Mean kurtosis and mean diffusivity values in tumor grading according to WHO-based histological findings and integrated molecular approach

| | n | $MK_n$ | $MD_n$ |
|---|---|---|---|
| WHO 2007-based findings | | | |
| Grade II/low grade glioma | 25 | 0.41 ± 0.09 | 1.86 ± 0.40 |
| Grade III glioma | 15 | 0.53 ± 0.11 | 1.48 ± 0.33 |
| Grade IV glioblastoma | 10 | 0.52 ± 0.11 | 1.59 ± 0.42 |
| High grade glioma (III–IV) | 25 | 0.52 ± 0.11 | 1.52 ± 0.36 |
| Astrocytoma | 22 | 0.46 ± 0.14 | 1.64 ± 0.42 |
| Oligodendroglioma | 4 | 0.43 ± 0.04 | 1.80 ± 0.58 |
| Oligoastrocytoma | 14 | 0.46 ± 0.09 | 1.79 ± 0.46 |
| Integrated molecular diagnosis | | | |
| Astrocytoma | 19 | 0.39 ± 0.11 | 1.96 ± 0.43 |
| Oligodendroglioma | 14 | 0.47 ± 0.05 | 1.65 ± 0.17 |
| Glioblastoma | 15 | 0.57 ± 0.10 | 1.39 ± 0.37 |
| Molecular characteristics | | | |
| IDH1/2 wild type in all tumors | 16 | 0.57 ± 0.09 | 1.43 ± 0.39 |
| IDH1/2 mutation in all tumors | 33 | 0.43 ± 0.09 | 1.82 ± 0.37 |
| IDH1/2 wild type in AS2, AS3, and GBM | 15 | 0.57 ± 0.10 | 1.41 ± 0.37 |
| IDH1/2 mutation in AS2, AS3, and GBM | 19 | 0.39 ± 0.11 | 1.96 ± 0.43 |
| ATRX maintained expression | 26 | 0.51 ± 0.10 | 1.56 ± 0.29 |
| ATRX loss of expression | 19 | 0.41 ± 0.11 | 1.90 ± 0.45 |
| 1p/19q lack of LOH | 23 | 0.46 ± 0.13 | 1.74 ± 0.45 |
| 1p/19q LOH | 12 | 0.47 ± 0.05 | 1.63 ± 0.25 |
| MGMT unmethylated | 15 | 0.48 ± 0.14 | 1.57 ± 0.48 |
| MGMT methylated | 19 | 0.50 ± 0.11 | 1.65 ± 0.33 |

Isocitrate-dehydrogenase (IDH) 1/2 mutation status; alpha-thalassemia/mental retardation syndrome X-linked (ATRX) expression; chromosome 1p/19q loss of heterozygosity (LOH); O6-methylguanine DNA methyltransferase (MGMT) promoter status, *MK_n/MDn* normalized mean kurtosis/diffusivity, *AS2* astrocytoma grade II, *AS3* astrocytoma grade III, *GBM* glioblastoma

MK metrics are dimensionless, MD [$10^{-3}$ mm$^2$/sec]

was no significant difference between $MK_n$ and $MD_n$ among tumors with a lack of or complete chromosome 1p/19q LOH, as well as those with an unmethylated or methylated MGMT promoter region. Regarding the integrated molecular diagnosis, $MK_n$ was significantly higher in primary glioblastoma (0.57 ± 0.10) than in astrocytoma (0.39 ± 0.11; p < 0.001) and oligodendroglioma (0.47 ± 0.05; p = 0.003), whereas $MK_n$ showed a non-significant tendency towards higher values in oligodendroglioma than in astrocytoma

(p = 0.1) (Fig. 2c). $MD_n$ was significantly higher in primary glioblastoma (1.96 ± 0.43) than in astrocytoma (1.39 ± 0.37, p = 0.001), whereas oligodendroglioma could not be differentiated from astrocytoma and oligodendroglioma (Fig. 2d). Significant p values are outlined in Fig. 2a–g. Exemplary ROC curves of significant differences are displayed in Fig. 2m–p. The figure includes the ROC AUC and optimal cutoff values. Finally, $MK_n$ and integrated molecular diagnoses were strongly positively correlated, $r_p(50) = 0.668$, p < 0.001, whereas $MK_n$ and conventional WHO-based tumor grades were only moderately positively correlated, $r_p(50) = 0.496$, p < 0.001. MIB-1 and $MK_n$ were moderately positively correlated, $r_p(44) = 0.492$, $r_p^2 = 0.242$, p = 0.001 (Fig. 2), whereas MIB-1 and $MD_n$ were weakly negatively correlated, $r_p(44) = -0.353$, $r_p^2 = 0.124$, p = 0.019.

## Discussion

The purpose of this study was to assess the diagnostic performance of DKI for in vivo molecular profiling of human glioma. According to the newly applied integrated molecular approach (Haarlem Consensus), $MK_n$ can differentiate between tumors classified as astrocytoma, oligodendroglioma, and glioblastoma through IDH1/2 mutation status and ATRX expression.

Inconsistent with Falangola et al. [28] and van Cauter et al. [2], we did not find a significant decrease in MK with age, and MD did not show a significant increase. Therefore, we decided not to correct the diffusion parameter values in the NAWM for age before normalization.

Lower MK values reflect the more homogeneous cell architecture and lower cell density in LGG, whereas HGG results in increased MK values due to increased cellularity, cellular heterogeneity, hemorrhage, necrosis, and microvascular proliferation [1, 30]. Our $MK_n$ values for G3G and GBM were significantly higher than for G2G. Also, the $MK_n$ values of HGG were significantly higher than in LGG. The results thus far confirm the values in the literature [2, 6, 13, 14]. The $MK_n$ and $MD_n$ values of our 10 GBM patients were heterogeneous. In 5 of these patients, the values were similar to those of G3G. Literature values of $MK_n$ for GBM were significantly higher than those for G3G and G2G [13, 14]. A possible reason for the discrepancy with the reported values could be found in the histopathological characteristics and proliferative activity of the GBM and the selection of the VOI in image analysis. Gliomas are heterogeneous tumor entities with potentially dissimilar morphologies as well as different grades of tumor cell density and proliferative activity [31, 32] "across different grades, within the same grade, and even within a single given tumor" [33]. In the 5 GBM patients with deviant $MK_n$ values, the histopathological slides with glioblastoma were reviewed and showed heterogeneous tumor areas with different grades of tumor cell density and proliferative activity. In 3 of these patients we found below average MIB-1 indices. Jiang et al. [14] reported that MK was strongly positively correlated with proliferative activity, and that MK was able to predict Ki-67 labeling index in 39%. In our study, $MK_n$ and proliferative activity were moderately positively correlated, and $MK_n$ could predict MIB-1 in only 24%. Therefore, $MK_n$ is not feasible as independent biomarker for reliably predicting MIB-1. However, the proliferative activity was routinely measured in a single tumor resection block, making the measurements highly susceptible to sampling bias. Because the VOI was drawn around each whole tumor in order to avoid sampling bias [26], it also included areas with lower tumor cell differentiation and proliferative activity than a "pure" GBM (i.e., the infiltrative border), which might have led to a decrease in average $MK_n$ values. Furthermore, our data

presented larger standard deviations of average $MK_n$ and $MD_n$ values in G2G and G3G than those presented in the literature [2, 6, 13, 14], implying a greater overlap between these two groups. One possible explanation could be the six "borderline" tumors between G2G and G3G with $MK_n$ and $MD_n$ results in between the corresponding average values. However, the DKI-based assessment of glioma grade seems to correlate more with the actual histopathological composition of each tumor than with only the conventional WHO-based tumor grades.

The combination of ATRX LOE and IDH1/2 mutation in the integrated approach characterizes diffuse astrocytoma, including its most aggressive histological subtype, GBM [18]. In the literature, GBM with IDH1 mutation is described as a "homogeneous group" of GBM with small cell morphology (i.e., lower cellular complexity) compared with the "heterogeneous presentation of more aggressive IDH1 wild-type" GBM [34]. Thus, lower $MK_n$ values reflect the more homogeneous cell architecture in integrated astrocytoma, whereas primary GBM shows increased $MK_n$ values due to increased cellularity, cellular heterogeneity, hemorrhage, necrosis, and microvascular proliferation [1, 30]. Our $MK_n$ values for primary GBM with IDH1/2 wild type and maintained ATRX expression were significantly higher than for integrated astrocytoma with IDH1/2 mutation and ATRX LOE, whereas the $MD_n$ values of primary GBM were significantly lower than in integrated astrocytoma. In isolation, $MK_n$ and $MD_n$ seem to be feasible biomarkers for predicting IDH1/2 mutation status and ATRX expression. The results thus far are consistent with previously-published results by Lee et al. [35], who found significant differences in MD between patients with the wild type and mutation of IDH1/2. However, the $MK_n$ values seem to correlate more with the integrated molecular diagnoses than with the conventional WHO-based tumor grades. Also, $MK_n$ appears to be superior to $MD_n$ for tumor grading, which corresponds with previous reports [2, 14].

All gliomas with 1p/19q LOH are considered as oligodendrogliomas, and an overwhelming majority is associated with maintained ATRX expression and IDH1/2 mutation [18]. In our study, all oligodendroglioma showed synchronous ATRX expression, IDH1/2 mutation, and 1p/19q LOH. Thus, both integrated GBM and oligodendroglioma share ATRX expression as a common feature, whereas both integrated astrocytoma and oligodendroglioma show IDH1/2 mutation. Glioma with 1p/19q LOH has been correlated with higher tumor cellularity [36], which would be reflected by higher $MK_n$ values and lower $MD_n$ values than IDH mutant astrocytoma [1, 30, 34]. Our $MK_n$ and $MD_n$ values of integrated oligodendroglioma were in between those of integrated astrocytoma and primary GBM. They could be significantly differentiated from those of integrated GBM, but not from those of integrated astrocytoma. Therefore,
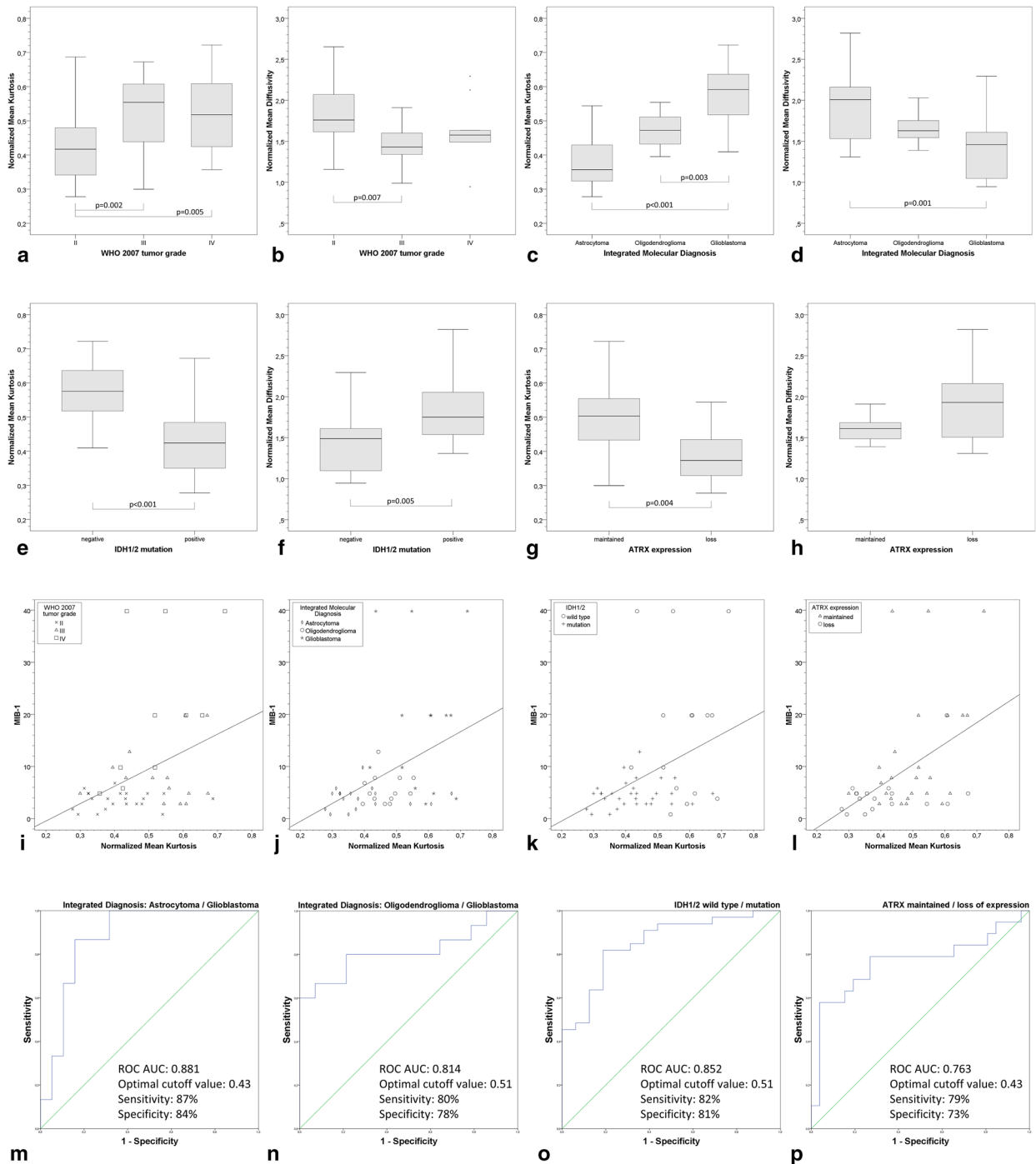
**Fig. 2** Mean kurtosis and mean diffusivity values as well as diagnostic performance in WHO-based tumor grading and integrated molecular approach. **a–h** Boxplots illustrate average $MK_n$ (**a, c, e, g**) and $MD_n$ (**b, d, f, h**) in tumor grading according to WHO-based histological findings (**a, b**), integrated diagnoses of astrocytoma, oligodendroglioma, and glioblastoma (**c, d**), IDH1/2 mutation status (**e, f**), and ATRX expression (**g, h**). Significant p values (**a–g**). **i–l** Scatter plots illustrate significant moderate positive correlation between MIB-1 and average $MK_n$ according to WHO-based tumor grades (**i**), integrated diagnoses of astrocytoma, oligodendroglioma, and glioblastoma (**j**), IDH1/2 mutation status (**k**), and ATRX expression (**l**). **m–p** AUC of ROC curves for discrimination between integrated molecular diagnoses of astrocytoma and glioblastoma (**m**), oligodendroglioma and glioblastoma (**n**), as well as between IDH1/2 mutation status (**o**), and maintained ATRX expression and LOE (**p**), based on $MK_n$ values. AUC and optimal cutoff values with corresponding sensitivity and specificity are displayed in the diagram. $MK_n$/$MD_n$ normalized mean kurtosis/diffusivity, *IDH* isocitrate-dehydrogenase, *ATRX* alpha-thalassemia/mental retardation syndrome X-linked, chromosome 1p/19q loss of heterozygosity (LOH), *MGMT* O6-methylguanine DNA methyltransferase, *AUC* Area under the curve, *ROC* Receiver operating characteristics, *MIB-1* Molecular immunology borstel (anti-Ki-67), MK is dimensionless, MD [$10^{-3}$ mm$^2$/sec]

$MK_n$ and $MD_n$ are not feasible as independent biomarkers for predicting chromosome 1p/19q LOH. However, future studies should further investigate the MK-based assessment of 1p/19q-confirmed oligodendroglioma.

MGMT can be regarded as an independent prognostic factor in patients with GBM [25]. MGMT promoter methylation increases responsiveness to temozolomide chemotherapy [19]. No MK or MD values for MGMT promoter status have been previously reported in the literature. However, we found no significant differences in MK and MD between tumors with unmethylated and methylated MGMT promoter.

## Limitations

One limitation of this study is a possible source of a selection bias in the slightly smaller group of WHO 2007 GBM patients with incoherent MK and MD values according to the literature. However, we found feasible explanations for this data. Furthermore, the measurements of proliferative activity (MIB-1) are possibly subject to sampling bias due to tumor heterogeneity.

## Conclusions

In the context of the upcoming integrated diagnostic approach combining histological and molecular data, DKI shows potential for differentiating between astrocytoma, oligodendroglioma, and primary GBM through IDH1/2 mutation status and ATRX expression. Considering the diagnostic and prognostic significance of these molecular markers, MK appears to be a promising in vivo biomarker for glioma. The diagnostic performance of MK and MD seems to fit better with the integrated molecular approach than the conventional histological findings of the current WHO 2007 classification.

## References

1. Louis DN, Ohgaki H, Wiestler OD et al (2007) The 2007 WHO classification of tumours of the central nervous system. Acta Neuropathol 114(2):97–109. doi:10.1007/s00401-007-0243-4

2. van Cauter S, Veraart J, Sijbers J et al (2012) Gliomas: diffusion kurtosis MR imaging in grading. Radiology 263(2):492–501. doi:10.1148/radiol.12110927

3. Scott JN, Brasher PMA, Sevick RJ et al (2002) How often are nonenhancing supratentorial gliomas malignant? A population study. Neurology 59(6):947–949

4. Watanabe M, Tanaka R, Takeda N (1992) Magnetic resonance imaging and histopathology of cerebral gliomas. Neuroradiology 34(6):463–469

5. Dean BL, Drayer BP, Bird CR et al (1990) Gliomas: classification with MR imaging. Radiology 174(2):411–415. doi:10.1148/radiology.174.2.2153310

6. van Cauter S, Keyzer F de, Sima DM et al (2014) Integrating diffusion kurtosis imaging, dynamic susceptibility-weighted contrast-enhanced MRI, and short echo time chemical shift imaging for grading gliomas. Neuro Oncol 16(7):1010–1021. doi:10.1093/neuonc/not304

7. Kulkarni AV, Guha A, Lozano A et al (1998) Incidence of silent hemorrhage and delayed deterioration after stereotactic brain biopsy. J Neurosurg 89(1):31–35. doi:10.3171/jns.1998.89.1.0031

8. Kärger J (1985) NMR self-diffusion studies in heterogeneous systems. Adv Colloid Interface Sci 23:129–148. doi:10.1016/0001-8686(85)80018-X

9. Jensen JH, Helpern JA, Ramani A et al (2005) Diffusional kurtosis imaging: the quantification of non-gaussian water diffusion by means of magnetic resonance imaging. Magn Reson Med 53(6):1432–1440. doi:10.1002/mrm.20508

10. Jensen JH, Helpern JA (2010) MRI quantification of non-Gaussian water diffusion by kurtosis analysis. NMR biomed 23(7):698–710. doi:10.1002/nbm.1518

11. Lu H, Jensen JH, Ramani A et al. (2006) Three-dimensional characterization of non-Gaussian water diffusion in humans using diffusion kurtosis imaging. NMR biomed 19(2): 236–247. doi:10.1002/nbm.1020

12. Poot DHJ, den Dekker AJ, Achten E et al (2010) Optimal experimental design for diffusion kurtosis imaging. IEEE Trans Med Imaging 29(3):819–829. doi:10.1109/TMI.2009.2037915

13. Raab P, Hattingen E, Franz K et al (2010) Cerebral gliomas: diffusional kurtosis imaging analysis of microstructural differences. Radiology 254(3):876–881. doi:10.1148/radiol.09090819

14. Jiang R, Jiang J, Zhao L et al (2015) Diffusion kurtosis imaging can efficiently assess the glioma grade and cellular proliferation. Oncotarget 6(39):42380–42393

15. Tan Y, Zhang H, Zhao R-F et al (2016) Comparison of the values of MRI diffusion kurtosis imaging and diffusion tensor imaging in cerebral astrocytoma grading and their association with aquaporin-4. Neurol India 64(2):265. doi:10.4103/0028-3886.177621

16. Louis DN, Perry A, Burger P et al (2014) International Society Of Neuropathology—Haarlem consensus guidelines for nervous system tumor classification and grading. Brain Pathol 24(5):429–435. doi:10.1111/bpa.12171

17. Reuss DE, Mamatjan Y, Schrimpf D et al (2015) IDH mutant diffuse and anaplastic astrocytomas have similar age at presentation and little difference in survival: a grading problem for WHO. Acta Neuropathol 129(6):867–873. doi:10.1007/s00401-015-1438-8

18. Reuss DE, Sahm F, Schrimpf D et al (2015) ATRX and IDH1-R132H immunohistochemistry with subsequent copy number analysis and IDH sequencing as a basis for an "integrated" diagnostic approach for adult astrocytoma, oligodendroglioma and glioblastoma. Acta Neuropathol 129(1):133–146. doi:10.1007/s00401-014-1370-3

19. Gerson SL (2004) MGMT: its role in cancer aetiology and cancer therapeutics. Nat Rev Cancer 4(4):296–307. doi:10.1038/nrc1319

20. Sahm F, Reuss D, Koelsche C et al (2014) Farewell to oligoastrocytoma: in situ molecular genetics favor classification as either oligodendroglioma or astrocytoma. Acta Neuropathol 128(4):551–559. doi:10.1007/s00401-014-1326-7

21. Capper D, Weissert S, Balss J et al (2010) Characterization of R132H mutation-specific IDH1 antibody binding in brain tumors. Brain Pathol 20(1):245–254. doi:10.1111/j.1750-3639.2009.00352.x

22. Schittenhelm J, Mittelbronn M, Meyermann R et al (2011) Confirmation of R132H mutation of isocitrate dehydrogenase 1 as an independent prognostic factor in anaplastic astrocytoma. Acta Neuropathol 122(5):651–652. doi:10.1007/s00401-011-0885-0

23. Hartmann C, Meyer J, Balss J et al (2009) Type and frequency of IDH1 and IDH2 mutations are related to astrocytic and oligodendroglial differentiation and age: a study of 1010 diffuse gliomas. Acta Neuropathol 118(4):469–474. doi:10.1007/s00401-009-0561-9

24. Thon N, Eigenbrod S, Grasbon-Frodl EM et al (2009) Novel molecular stereotactic biopsy procedures reveal intratumoral homogeneity of loss of heterozygosity of 1p/19q and TP53 mutations in World Health Organization grade II gliomas. J Neuropathol Exp Neurol 68(11):1219–1228. doi:10.1097/NEN.0b013e3181bee1f1

25. Hegi ME, Diserens A-C, Gorlia T et al (2005) MGMT gene silencing and benefit from temozolomide in glioblastoma. N Engl J Med 352(10):997–1003. doi:10.1056/NEJMoa043331

26. Tozer DJ, Jäger HR, Danchaivijitr N et al (2007) Apparent diffusion coefficient histograms may predict low-grade glioma subtype. NMR Biomed 20(1):49–57. doi:10.1002/nbm.1091

27. Kang Y, Choi SH, Kim Y-J et al (2011) Gliomas: histogram analysis of apparent diffusion coefficient maps with standard- or high-b-value diffusion-weighted MR imaging—correlation with tumor grade. Radiology 261(3):882–890. doi:10.1148/radiol.11110686

28. Falangola MF, Jensen JH, Babb JS et al (2008) Age-related non-Gaussian diffusion patterns in the prefrontal brain. J Magn Reson Imaging 28(6):1345–1350. doi:10.1002/jmri.21604

29. Coutu JP, Chen JJ, Rosas HD et al (2014) Non-Gaussian water diffusion in aging white matter. Neurobiol Aging 35(6):1412–1421. doi:10.1016/j.neurobiolaging.2013.12.001

30. Kleihues P, Soylemezoglu F, Schauble B et al (1995) Histopathology, classification, and grading of gliomas. Glia 15(3):211–221. doi:10.1002/glia.440150303

31. Soeda A, Hara A, Kunisada T et al (2015) The evidence of glioblastoma heterogeneity. Sci Rep 5: 7979. doi:10.1038/srep07979

32. DeAngelis LM (2001) Brain tumors. N Engl J Med 344(2):114–123. doi:10.1056/NEJM200101113440207

33. Cha S (2006) Update on Brain Tumor Imaging: From Anatomy to Physiology. AJNR Am J Neuroradiol 27(3):475–487

34. Popov S, Jury A, Laxton R et al (2013) IDH1-associated primary glioblastoma in young adults displays differential patterns of tumour and vascular morphology. PLoS One 8(2):e56328. doi:10.1371/journal.pone.0056328

35. Lee S, Choi SH, Ryoo I et al (2015) Evaluation of the microenvironmental heterogeneity in high-grade gliomas with IDH1/2 gene mutation using histogram analysis of diffusion-weighted imaging and dynamic-susceptibility contrast perfusion imaging. J Neurooncol 121(1):141–150. doi:10.1007/s11060-014-1614-z

36. Kim SH, Kim H, Kim TS (2005) Clinical, histological, and immunohistochemical features predicting 1p/19q loss of heterozygosity in oligodendroglial tumors. Acta Neuropathol 110(1):27–38. doi:10.1007/s00401-005-1020-x